# ESM of Li-ion Conductive Materials for Energy Generation and Storage

*Roger Proksch, Asylum Research*

*Nina Balke, Stephen Jesse and Sergei Kalinin, Oak Ridge National Laboratory*

## Introduction

Electrochemical strain microscopy (ESM) is a novel scanning probe microscopy (SPM) technique for the **Cypher**™ and **MFP-3D**™ Atomic Force Microscopes (AFMs) that is capable of probing electrochemical reactivity and ionic flows in solids with unprecedented resolution. ESM's capabilities are invaluable for investigating and improving performance for a broad range of energy technologies, including batteries and fuel cells for electric vehicles and grid storage. This note describes applications of ESM for Li-ion electrolytes and cathode and anode materials.

The capability to probe electrochemical processes and ionic transport in solids is invaluable for a broad range of applications for energy generation and storage, including batteries[1,2] and fuel cells.[3,4,5] The viability of electric vehicles and grid storage as key components of renewable energy technology hinges on advances in battery energy densities and lifetimes. Progress in these areas requires understanding of materials' electrochemical functionality on the sub-micron and nanometer level of individual particles and structural elements. As some examples, consider that semiconductor devices are expected to undergo billions of operation cycles, and structural materials used in aircraft or nuclear reactor vessels require fail-safe functioning for decades. For comparison, the fading (irreversible capacity loss) of current Li-ion batteries begins after only hundreds of operational cycles (Figure 1).[6]

The reason for such disparity between lifetimes for energy and structural/semiconductor materials is that the functionality of energy materials is not fully understood or controlled below the device level. In comparison, the functionality of semiconductors and structural materials is well understood on the level of single defects, allowing for predictive modeling and materials design. Although the structure of energy materials can be ascertained from atomic to macroscopic levels, electrochemical properties below the device level remain an enigma. For example, while defects or interfaces can be observed by electron microscopy, their specific roles in interfacial reaction, electronic or ionic transport, and strain relaxation cannot currently be determined. Only after understanding of electrochemical functionality on the level of individual nanoparticles or structural defects is available can practical, knowledge-driven research and development proceed. Electrochemical Strain Microscopy (ESM) has the potential to aid in these advances with two major improvements over other current technologies: (a) the resolution to probe nanometer-scale volumes and (b) imaging capability extended to a broad range of spectroscopic techniques. The following examples describe applications of ESM for imaging and spectroscopic methods.

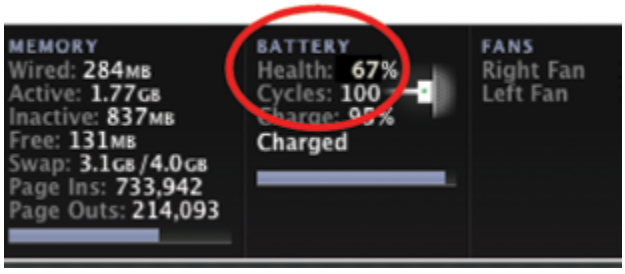


*Figure 1: Toolbar from a laptop showing a fading "Health" of a Li-ion battery after only 100 cycles.*

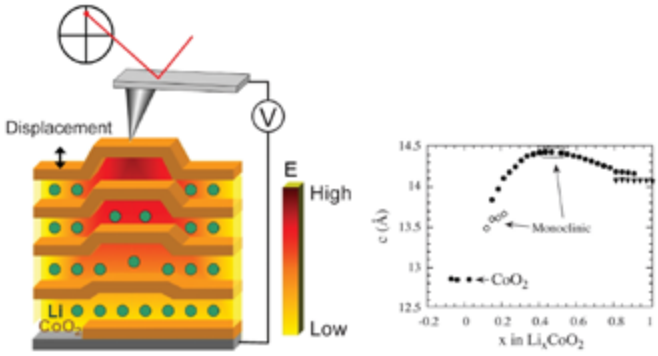


*Figure 2: Principle of Electrochemical Strain Microscopy. (a) During ESM, a periodic bias is applied to the SPM tip in contact with the sample surface. The applied bias induces ionic motion in the sample and the resulting surface deformation is detected by the SPM probe and electronics, generating an image that maps the ionic motion at the nanoscale. (b) The dependence of the c-lattice parameter (perpendicular to layers) on lithiation in prototypical $LixCoO_2$ cathode material.[10] In the operation region of Li-ion batteries (from x = 1 to x=0.5), the lattice parameter changes linearly with x by 40 pm. Combined with the ~1 pm sensitivity limit of the Cypher AFM, this suggests that a lithiation state change of just 10% can be measured through 1 unit cell of material.*

OXFORD INSTRUMENTS

*The Business of Science®*

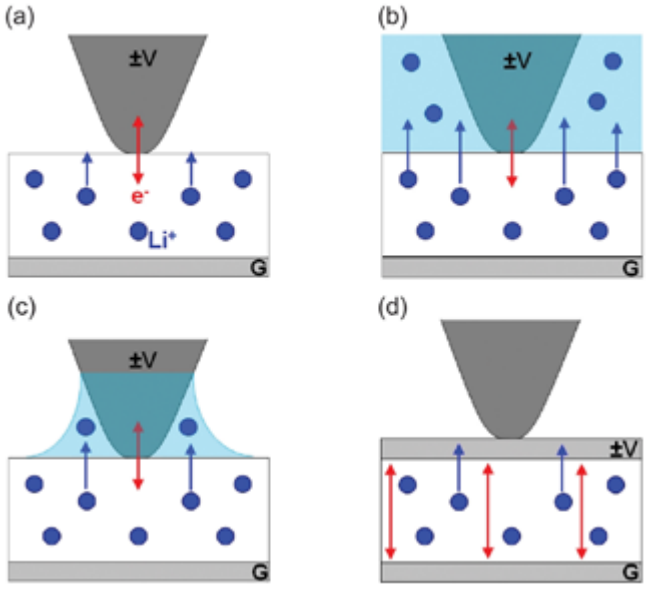


*Figure 3: Operational regimes for electrochemical strain microscopy. (a) a blocking tip electrode (low humidity or vacuum) (b) Li-containing electrolyte (c) ambient conditions with a liquid droplet at the tip-surface and (d) on the surface of the top-electrode device. See text for more details.*

ESM,[7] conceptually illustrated in Figure 2, is a novel scanning probe microscopy (SPM) technique capable of probing electrochemical reactivity and ionic flows in solids on the sub-ten-nanometer level,[8] three to four orders of magnitude below the effective resolution of conventional electrochemical methods. Comparative analysis of SPM methods for probing electrochemical processes in solids is given here.[9] While scanning tunneling microscopes (STMs) measure electronic currents and atomic force microscopy (AFM) measures *forces*, ESM is the first technique that measures the direct coupling of *ionic* currents to strain (or position) measurements, providing a new tool for mapping electrochemical phenomena on the nanoscale.

ESM is based on detecting the strain response of a material to an applied electric field though a blocking or electrochemically active SPM tip (a tip that is functionalized directly or placed in an ion-containing medium). A biased SPM tip concentrates an electric field in a nanometer-scale volume of material, inducing interfacial electrochemical processes at the tip-surface junction and ionic currents through the solid.[11] The intrinsic link between concentration of ionic species and/or oxidation states of the host cation and the molar volume of the material results in electrochemical strain and surface displacement. This is the case for many ionic and mixed ionic-electronic conductors such as ceria,[12] cobaltites,[13,14,15,16] nikelates[17] and manganites,[18] etc. Similarly, insertion and extraction of Li-ions in Li-battery electrodes produce large volume changes.[19,20] The sensitivity of a platform such as the Cypher AFM allows for detection of ~1 picometer (pm = $10^{-3}$ nm = or $10^{-12}$ m) surface displacements in the ~0.1 to 1 MHz frequency range, which allows a theoretical detection limit of approximately 10% changes in lithiation state within one unit cell (i.e., elementary volume of material) for materials such as $LiCoO_2$ (one of the most common cathode components). This is in a 1 kHz imaging bandwidth.

There are a number of different operational regimes for electrochemical strain microscopy, schematically described in Figure 3. Figure 3(a) shows a blocking tip electrode, where the electron transfer between tip and surface and the non-uniform electrostatic field result in mobile ion redistribution within the solid but no electrochemical process at the interface. Figure 3(b) shows ESM being performed in liquid Li-containing electrolyte – even for finite electronic conductivities, the ac electric field is concentrated in the tip-surface junction. Figure 3(c) shows the situation in ambient conditions, where the formation of a liquid droplet at the tip-surface junction provides a Li-ion reservoir, rendering electrodes partially reversible. A similar effect can occur for blocking electrodes at high biases (Li-extraction and tip plating) or for Li-electrolyte-coated electrodes. Finally, Figure 3(d) shows ESM being performed on the surface of the top-electrode device, where both the ionic currents are limited by the cathode and anode. In the cases shown in (a) and (b), the electric field created by the probe is localized, in (d) the field is uniform, and in (c) the field localization is controlled by solution conductivity and modulation frequency. In all cases, the tip detects local strain induced by the local or nonlocal electric field.

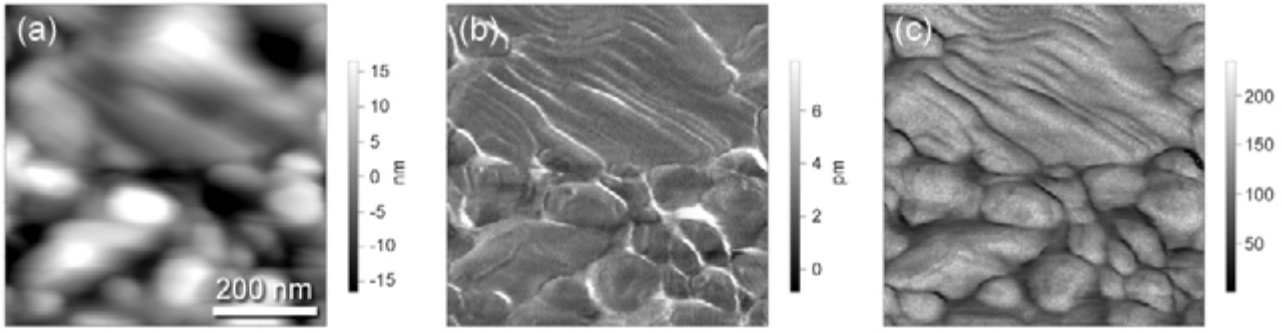


*Figure 4: (a) Topography, (b) ESM amplitude and (c) quality factor (dissipation) of a $LiCoO_2$ cathode imaged on an MFP-3D AFM using DART.*

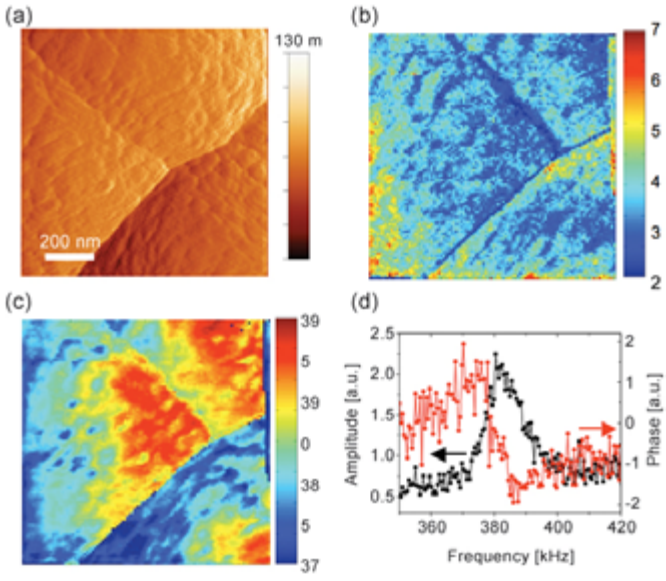


*Figure 5: Mapping of the electrochemical strain response in a Si anode. (a) Deflection signal of a 1×1 μm area showing a triple boundary point. (b) Contact resonance amplitude, and (c) resonance frequency map showing heterogeneous strain response and a strong correlation between resonance frequency and topography. (d) A single-point contact resonance peak from the boundary region. The data was acquired in BE mode (adapted from reference 8).*

In general, the use of high frequencies in electromechanical SPM (including piezoresponse force microscopy)[21] allows one to effectively employ cantilever resonances that can amplify small surface oscillations by a factor of 10 to 100 while avoiding the 1/f noise corner of the optical detection system (~10 kHz). To avoid crosstalk with surface topography, we use the Band Excitation (BE) method, recently developed at ORNL and Asylum,[22] and the dual AC resonance tracking method (DART), developed at Asylum and ORNL.[23] In BE, the excitation and detection are performed using a signal with defined amplitude and phase content over a given frequency interval. The BE approach allows mapping of the resonant frequency (which provides information similar to that obtained by atomic force acoustic microscopy), local quality factor, and response amplitude – all of which are measurements directly related to electrochemical activity.

In DART, the amplitude-based feedback is used to track cantilever resonance and its quality factor,[24] providing information similar to BE. The use of BE and DART methods allows effective use of cantilever resonant amplification and obviates the indirect topographic cross-talk inevitable in single-frequency SPMs.[25] The DART technique is a standard feature in Asylum's IGOR-based software[26], while BE is currently only available to ORNL and their collaborators.[26]

To date, ESM has been demonstrated (see Figure 4 for example) for a variety of lithium-ion materials (including layered transition metal oxide cathodes,[11] silicon anodes,[8,27] and electrolytes such as LISICON), oxygen electrolytes (including yttria-stabilized zirconia [YSZ] and samarium-doped ceria), mixed electronic-ionic conductors for fuel cell cathodes, and some proton conductors. Theoretical principles of ESM are considered in several recent publications.[28,29,30,31] In addition, because electrochemical strains are ubiquitous in virtually all solid-state ionics, ESM will be applicable to all battery and fuel cell materials.

The remarkable aspect of the strain detection in ESM, as opposed to current-based techniques, is that the signal originates only from strains induced by ion motion, whereas electric currents contain (and are often dominated by) contributions from electronic conduction (direct current) and double-layer and instrumental capacitances. The fact that ionic diffusion is intrinsically slow, and hence the ionic currents are intrinsically small, imposes very significant and stringent limitations on current detection. While this is also relevant to strain detection, the simple analysis of the detection limits suggests that electrochemical strains can be measured in volumes $10^6$ to $10^8$ times smaller than Faradaic currents.[27,28] The high-resolution (<10 nm) data shown in Figure 5 clearly demonstrate this for a Si anode sample.

## Vector ESM

As is the case with PFM measurements, the three-dimensional surface displacement in ESM can be characterized with cantilever deflection and torsion measurements (Figure 6). The evolution from purely vertical (out-of-plane, OP) to purely lateral (in-plane, IP) surface displacements is shown going from left to right in the figure. For the IP and OP signals shown in Figure 7, the ESM signals are recorded around the deflection and torsional resonance frequencies of the cantilever at 360 KHz and 710 kHz, respectively. These frequencies are determined by the mechanical properties of the cantilever and the cantilever-sample contact and were determined using the BE method. The measured parameters are the maximum surface oscillation (height of the contact resonance peak) which forms the ESM signal.

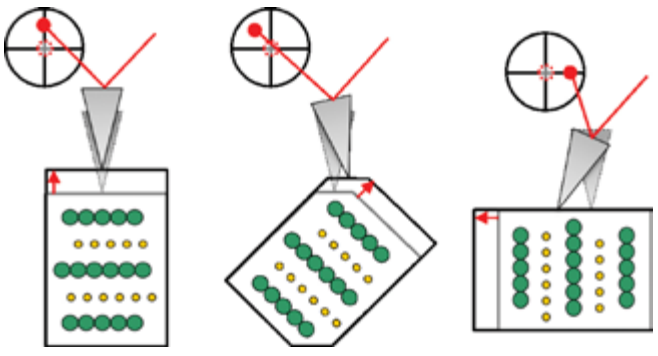

*Figure 6: Correlation between OP and IP ESM response and the grain orientation.*

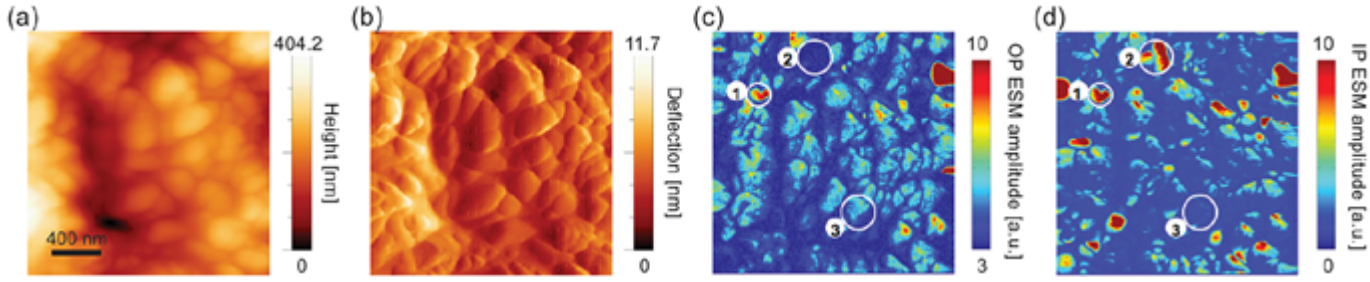


*Figure 7: (a) Topography, (b) deflection, (c) OP ESM map, (d) IP ESM map for a 2x2 µm area on a $LiCoO_2$ thin film.*

Figure 7 displays the correlation between topography and the measured OP and IP ESM amplitude and phase signals. To demonstrate the surface characteristics of the $LiCoO_2$ film, topography and deflection signals are shown in Figure 7(a) and 7(b), respectively. Small grains of $LiCoO_2$ with a diameter of approximately 200-300 nm can be identified. The maximum OP and IP ESM amplitudes are displayed in Figure 7(c) and 7(d). Both images show strong variations in the ESM response across the scanned area. In addition, the OP and IP ESM amplitude map do not show the same features, demonstrating no or minimum cross-talk between the cantilever deflection and torsion. If Figure 7(c) and 7(d) are compared, grains with OP and IP response (#1), no OP but IP response (#2), and OP but no IP response (#3) can be identified.

As is the case with PFM measurements, the three-dimensional surface displacement in ESM can be characterized with cantilever deflection and torsion measurements (Figure 6). The evolution from purely vertical (out-of-plane, OP) to purely lateral (in-plane, IP) surface displacements is shown going from left to right in the figure. For the IP and OP signals shown in Figure 7, the ESM signals are recorded around the deflection and torsional resonance frequencies of the cantilever at 360 KHz and 710 kHz, respectively. These frequencies are determined by the mechanical properties of the cantilever and the cantilever-sample contact and were determined using the BE method. The measured parameters are the maximum surface oscillation (height of the contact resonance peak) which forms the ESM signal.

Figure 7 displays the correlation between topography and the measured OP and IP ESM amplitude and phase signals. To demonstrate the surface characteristics of the $LiCoO_2$ film, topography and deflection signals are shown in Figure 7(a) and 7(b), respectively. Small grains of $LiCoO_2$ with a diameter of approximately 200-300 nm can be identified. The maximum OP and IP ESM amplitudes are displayed in Figure 7(c) and 7(d). Both images show strong variations in the ESM response across the scanned area. In addition, The OP and IP ESM amplitude map do not show the same features, demonstrating no or minimum cross-talk between the cantilever deflection and torsion. If Figure 7(c) and 7(d) are compared, grains with OP and IP response (#1), no OP but IP response (#2), and OP but no IP response (#3) can be identified.

## Time Spectroscopy

ESM signals can be used as a basis for a broad set of voltage and time spectroscopies. The spectroscopic techniques in ESM have been developed following the protocols of classical electrochemical methods (e.g. potentiostatic intermittent titration, galvanostatic intermittent titration, electrochemical impedance spectroscopy), in which the local electrochemical strain signal substitutes for macroscopic Faradaic currents. Once properly calibrated, these techniques offer potential for implementation of the rich panoply of electrochemical techniques on the nanoscale level in a spatially-resolved fashion.

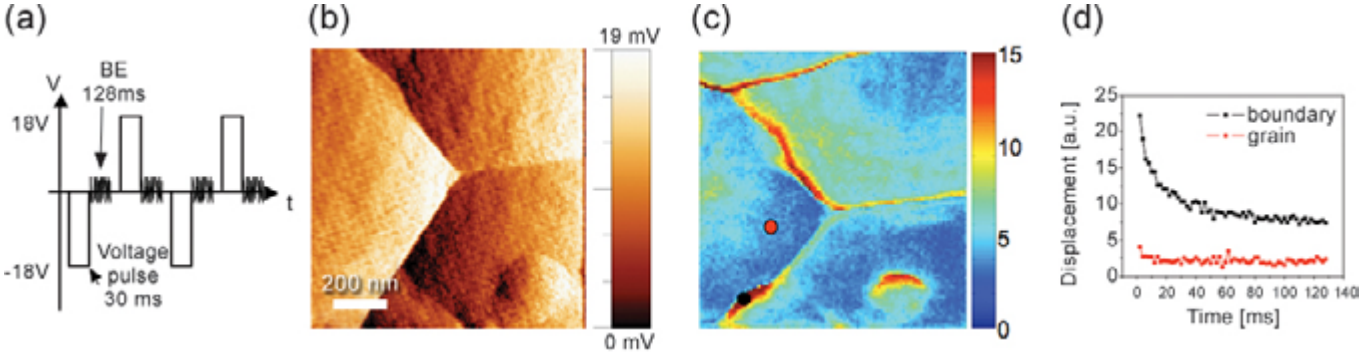


*Figure 8: Mapping of Li-ion relaxation. (a) Scheme of voltage pulses applied to measure relaxation maps. (b) Deflection signal of a 1×1 µm area showing grain boundaries. (c) Map of maximum displacement measured after -18 V voltage pulse of 30 ms length. (d) Single-point relaxation curves from two points in the map as indicated.*

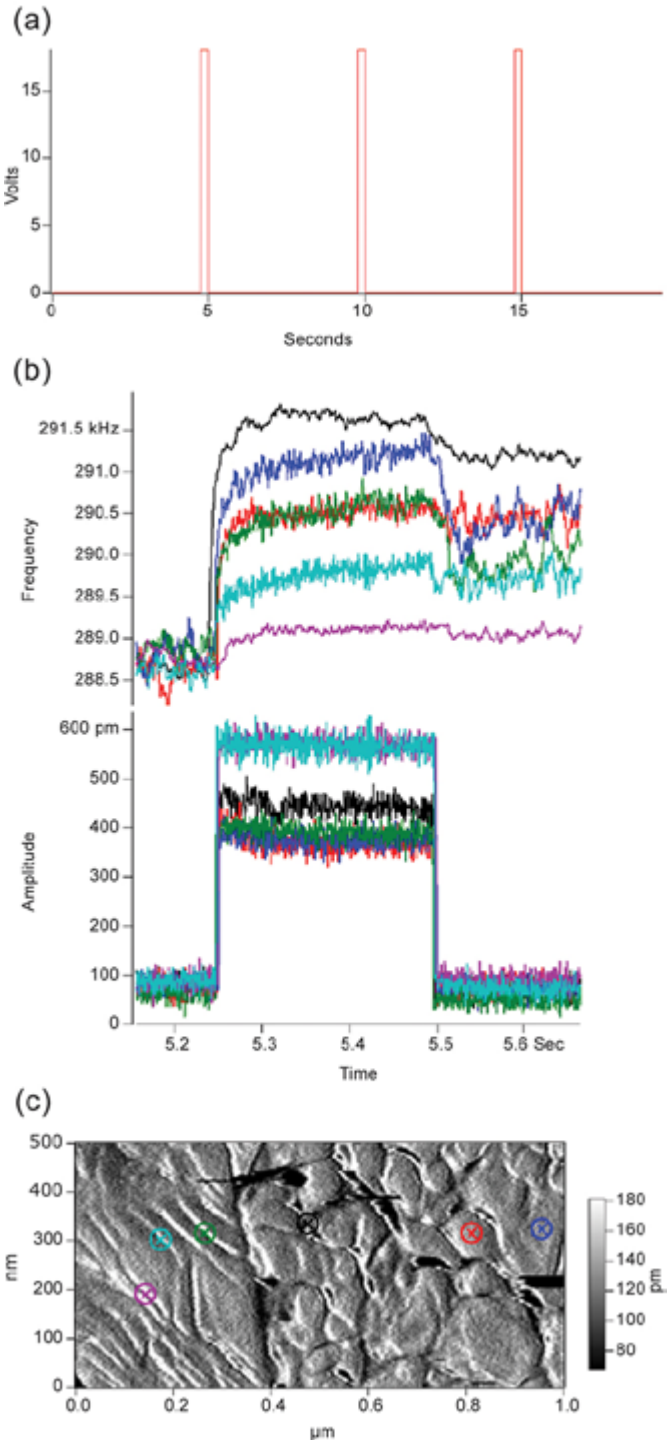


*Figure 9: Point-by-point DART Mapping of Li-ion relaxation. (a) Voltage pulses applied to measure relaxation, and (b) contact resonance Frequency and Amplitude signals made at color-coded location on the (c) sample topography of a 1×0.5 µm area showing grain boundaries.*

In ESM time spectroscopy, the signal is measured after the application of a single voltage pulse to the probe, and the response is measured over a long time (ideally, comparable to the diffusion time of Li ions). In the mapping mode, the relaxation curves are measured over an array, and the characteristic parameters (relaxation times, relaxation amplitude) can be measured in a spatially resolved fashion across the sample surface. Remarkably, in addition to measuring the relaxation time, the diffusion length can often be determined from spatially resolved images, thus allowing quantitative determination of the diffusion coefficient. This spectroscopic method is reminiscent of the well-known potentiostatic and galvanostatic intermittent titration techniques[32,33,34,35] but performed on the nanometer scale (Figures 8 and 9).

## Voltage spectroscopy and reaction-diffusion separation

As an alternative to the time spectroscopy described above, voltage spectroscopic measurements can be performed as well. In this case, voltage pulses of increasing and decreasing amplitude are applied to the probe, and the electrochemical strain response is tested after each pulse. The voltage sweep provides the advantage of faster measurements (compared to time spectroscopy, where only one voltage is tested at a time) and also includes information about Li-ion diffusion and concentration in the probed volume (Figure 10).

Electrochemical processes typically are composed of several interfacial reaction and diffusion steps. A reaction is typically exponentially dependent on overpotential while diffusion changes linearly with driving force. Consequently, for low potentials the process is limited by reaction, while for high potentials it is limited by diffusion. Correspondingly, measuring the ESM signal as a function of bias pulse magnitude allows differentiation of the reaction and diffusion.[8]

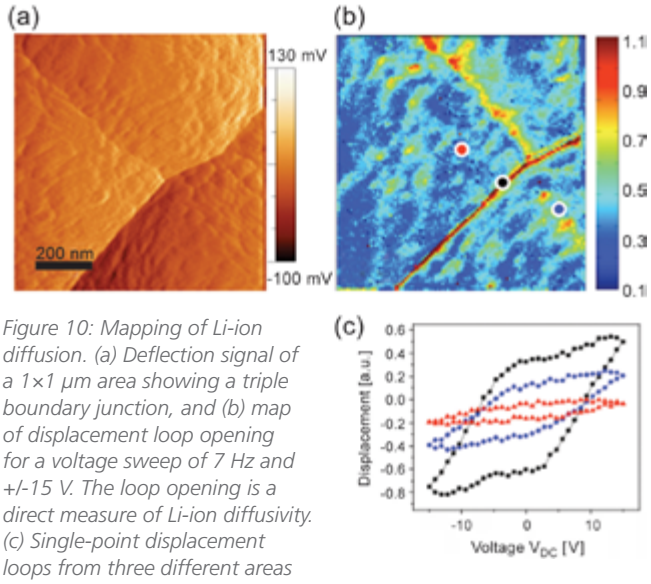


*Figure 10: Mapping of Li-ion diffusion. (a) Deflection signal of a 1×1 µm area showing a triple boundary junction, and (b) map of displacement loop opening for a voltage sweep of 7 Hz and +/-15 V. The loop opening is a direct measure of Li-ion diffusivity. (c) Single-point displacement loops from three different areas as indicated in B (adapted from reference 8).*

## Combining ionic and electron current imaging

Complementary information on electronic transport properties can be obtained from conductive AFM.[36,37,38,39,40,41] On the MFP-3D and Cypher platforms, the conductive AFM measurements are implemented using ORCA,™ a trans-impedance amplifier that places the cantilever at a virtual ground. In contrast to "standard" ESM imaging, this means that the sample support is driven with the oscillating voltages and biases. The circuit configuration is shown in Figure 11. An example of this combined imaging technique is shown in Figure 12 where the ionic conductivity as measured by ESM is contrasted with the electronic transport in a $LiCoO_2$ cathode.

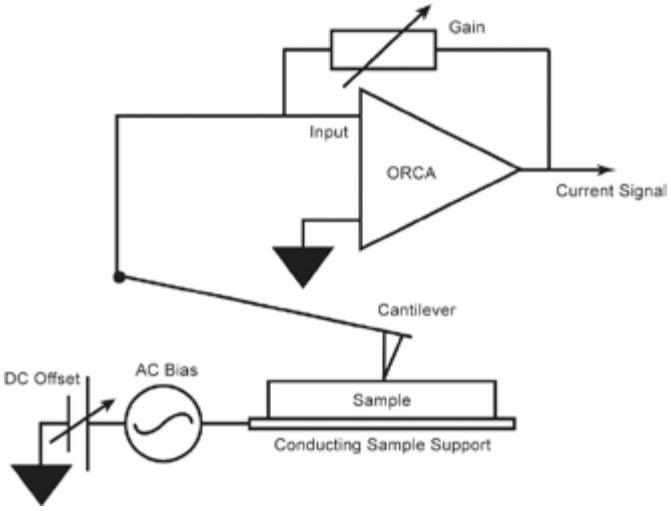


*Figure 11: Electrical connections for simultaneous Current (ORCA) and ESM measurements. The cantilever deflection is measured in the usual manner while the Current signal can be plotted as a function of position, DC Offset, AC Bias etc.*

## Summary

The capability for probing electrochemical processes and ionic transport in solids is invaluable for the study and improvement of a broad range of energy technologies and applications, including batteries and fuel cells. The viability of electric vehicles and grid storage as key components of renewable-energy technology hinges on advances in battery energy densities and lifetimes. However, the progress in this field has been limited by an almost complete lack of tools capable of probing local electrochemical activity on the nanoscale. While the behavior of the assembled device can be explored, the functionality of its parts cannot. Correspondingly, progress in the electrochemical industry (e.g., power and energy density vs time) has been significantly slower than in, for example, semiconductor and information technologies, with development of the former largely driven by trial and error.

Electrochemical Strain Microscopy is a technique capable of probing electrochemical reactivity and ionic flows in solids on the sub-ten-nanometer level. This method utilizes the intrinsic link between electrochemical processes and strains, as opposed to Faradaic current detection in classical electrochemical methods. This different and unique detection principle allows electrochemical measurements in nanometer-scale volumes that can be extended to a broad spectrum of time and voltage spectroscopies. It is anticipated that ESM will be a key analytical capability for investigating and improving performance of energy storage devices.

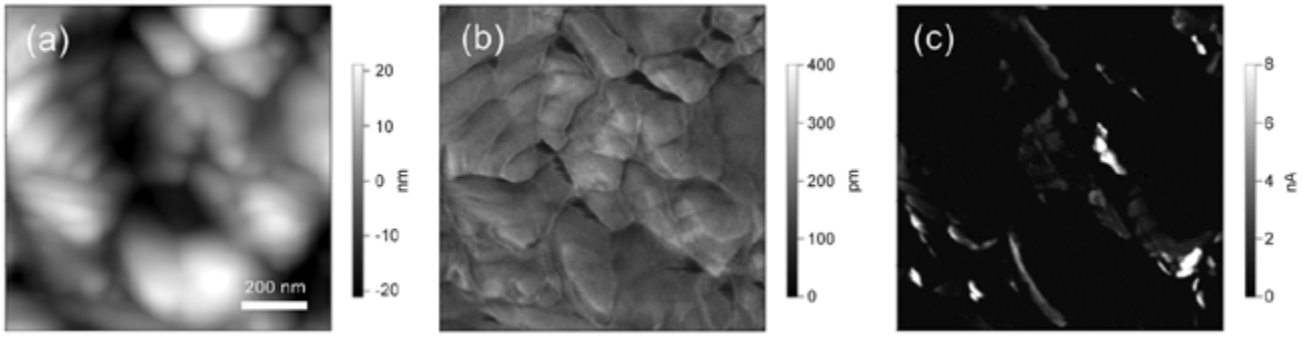


*Figure 12: Simultaneous DART and ORCA images of a $LiCoO_2$ cathode made with an AC Bias of 0.2 V and a DC Offset of 1 V. (a) shows the topography (b) shows the ESM amplitude, dependent on the ionic current, and (c) shows the DC current measured with the ORCA module. This image in particular underscores the lack of correlation between the ionic and electronic current flow in the sample.*

## References


1. R.A.Huggins, Advanced Batteries: Materials Science Aspects (Springer-Verlag, New York, 2008).
2. G.A. Nazri, & G. Pistoia, (Eds.) Lithium Batteries: Science and Technology (Springer-Verlag, New York, 2009).
3. R. O'Hayre, S.W. Cha, W. Colella, F.B. Prinz, Fuel Cell Fundamentals, John Wiley & Sons, New York, 2009.
4. V.S. Bagotsky, Fuel Cells: Problems and Solutions, Wiley 2009.
5. R. O'Hayre, Probing Electrochemistry at the Micro Scale: Applications in Fuel Cells, Ionics, and Catalysis, VDM Verlag, Saarbruecken, 2008.
6. M. Armand, J.M. Tarascon, Key challenges in future Li-battery research, *Nature* **451**, 652 (2008).
7. S.V. Kalinin, N. Balke, A. Kumar, N.J. Dudney, S. Jesse, "Real Space Mapping of Ionic Diffusion and Electrochemical Activity in Energy Storage and Conversion Materials" U.S. Patent pending.
8. N. Balke, S. Jesse, Y. Kim, L. Adamczyk, A. Tselev, I.N. Ivanov, N.J. Dudney, and S.V. Kalinin, Real Space Mapping of Li-Ion Transport in Amorphous Si Anodes with Nanometer Resolution, *Nano Lett* **10**, 3420 (2010).
9. S.V. Kalinin and N. Balke, Local electrochemical functionality in energy storage materials and devices by scanning probe microscopies: status and perspectives, *Adv. Mat.* **22**, E193 (2010).
10. G.G. Amatucci, J.M. Tarascon, & L.C. Klein, $CoO_2$, the end member of the $LixCoO_2$ solid solution. J. *Electrochem. Soc.* **143**, 1114-1123 (1996).
11. N. Balke, S. Jesse, A.N. Morozovska, E. Eliseev, D.W. Chung, Y. Kim, L. Adamczyk, R.E. Garcia, N. Dudney, and S.V. Kalinin, *Nature Nanotechnology* **5**, 749 (2010)
12. S.R. Bishop, K.L. Duncan and E.D. Wachsman, *Electrochimica Acta* **54**, 1436 (2009).
13. S.B. Adler. *J. Am. Ceram Soc.* **84**, 2117 (2001).
14. A.Y. Zuev, A.I. Vylkov, A.N. Petrov, D.S. Tsvetkov, *Solid State Ionics* **179**, 1876 (2008).
15. H.L. Lein, K. Wiik and T. Grande. *Solid State Ionics* **177**, 1795 (2006).
16. Xiyong Chen, Jinsong Yu, and S.B. Adler, *Chem. Mater.* **17**, 4537 (2005).
17. V.V. Kharton, A.V. Kovalevsky, M. Avdeev, E.V. Tsipis, M.V. Patrakeev, A.A. Yaremchenko, E.N. Maumovich, J.R Frade, *Chem. Mater.* **19**, 2027 (2007).
18. A.Yu. Zuev, D.S. Tsvetkov, *Solid State Ionics* **181**, 557 (2010).
19. Y. T. Cheng, M.W. Verbrugge, *J. Power Sources* **190**, 453 (2009).
20. X. Zhang, A.M. Sastry, W. Shyy, *J. Electrochem. Soc.* **155**, A542 (2008).
21. R. Proksch and S.V. Kalinin, Asylum Research Application Note 10 - Piezoresponse Force Microscopy with Asylum Research AFMs.
22. S. Jesse, S.V. Kalinin, R. Proksch, A.P. Baddorf, and B.J. Rodriguez, Energy Dissipation Measurements on the Nanoscale: Band Excitation Method in Scanning Probe Microscopy, *Nanotechnology* **18**, 435503 (2007).
23. B.J. Rodriguez, C. Callahan, S.V. Kalinin, and R. Proksch, Dual-Frequency Resonance-Tracking Atomic Force Microscopy, *Nanotechnology* **18**, 475504 (2007).
24. A. Gannepalli, D. Yablon, A. Tsou and R. Proksch, Mapping nanoscale elasticity and dissipation using dual frequency contact resonance AFM, *Nanotechnology* **22**, 355705 (2011).
25. S. Jesse, S. Guo, A. Kumar, B.J. Rodriguez, R. Proksch and S.V. Kalinin, Resolution theory and static- and frequency dependent cross-talk in piezoresponse force microscopy, *Nanotechnology* **21**, 405703 (2010).
26. https://afm.oxinst.com/PFM
27. N. Balke, S. Jesse, Y. Kim, L. Adamczyk, I.N. Ivanov, N.J. Dudney, and S.V. Kalinin, Decoupling electrochemical reaction and diffusion processes in ionically-conductive solids on the nanometer scale, *ACS Nano* **4**, 7349 (2010).
28. A. Morozovska, E. Eliseev, and S.V. Kalinin, Electromechanical Probing of Ionic Currents in Energy Storage Materials, *Appl. Phys. Lett.* **96**, 222906 (2010).
29. A. Morozovska, E. Eliseev, N. Balke, and S.V. Kalinin, Local probing of ionic diffusion by electrochemical strain microscopy: spatial resolution and signal formation mechanisms, *J. Appl. Phys.* **108**, 053712 (2010).
30. A.N. Morozovska, E.A. Eliseev, A.K. Tagantsev, S. Bravina, L.Q. Chen, and S.V. Kalinin, Thermodynamics of electromechanically coupled mixed ionic-electronic conductors: Deformation potential, Vegard strains, and flexoelectric effect, *Phys. Rev. B* **83**, 195313 (2011).
31. A.N. Morozovska, E.A. Eliseev, G.S. Svechnikov, and S.V. Kalinin, Nanoscale Electromechanics of Paraelectric Materials with Mobile Charges: Size effects and Nonlinearity of Electromechanical Response of $SrTiO_3$ Films, *Phys. Rev. B* **84**, 045402 (2011).
32. A.J. Bard and L.R. Faulkner, Electrochemical Methods: Fundamentals and Applications, John Wiley & Sons, New York (2001).
33. J.S. Newman, Electrochemical Systems, Prentice Hall, New Jersey (1980).
34. C.J. Wen, B.A. Boukamp, R.A. Huggins, W.J. Weppner,

*Electrochem. Soc.* **1979**, 126, 2258-2266.

35. W. Weppner, R.A. Huggins, *Annu. Rev. Mat. Sci.* **1978**, 8, 269-311.
36. R. Kostecki, F. Kong, Y. Matsuo, and F. McLarnon, Interfacial studies of a thin-film $Li_2Mn_4O_9$ electrode, *Electrochim. Acta* **45**, 225 (1999).
37. Y. Matsuo, R. Kostecki, and F. McLarnon, Surface layer formation on thin-film $LiMn_2O_4$ electrodes at elevated temperatures, *J. Electrochem. Soc.* **148**, A687 (2001).
38. R. Kostecki and F. McLarnon, Local-probe studies of degradation of composite $LiNi_{0.8}Co_{0.1}5Al_{0.05}O_2$ cathodes in high-power lithium-ion cells, *Electrochem. Solid-State Lett.* **7**, A380 (2004).
39. T.M. McEvoy and K.J. Stevenson, Spatially resolved imaging of inhomogeneous charge transfer behavior in polymorphous molybdenum oxide. I. Correlation of localized structural, electronic, and chemical properties using conductive probe atomic force microscopy and raman microprobe spectroscopy, *Langmuir* **21**, 3521 (2005).
40. T.M. McEvoy and K.J. Stevenson, Spatially resolved imaging of inhomogeneous charge transfer behavior in polymorphous molybdenum oxide. II. Correlation of localized coloration/insertion properties using spectroelectrochemical microscopy, *Langmuir* **21**, 3529 (2005).
41. D.A. Bussian, J.R. O'Dea, H. Metiu, and S.K. Buratto, Nanoscale current imaging of the conducting channels in proton exchange membrane fuel cells, *Nano Lett.* **7**, 227 (2007).

This research (SVK, NB, SJ) was conducted in part at the Center for Nanophase Materials Sciences, which is sponsored at Oak Ridge National Laboratory by the Office of Basic Energy Sciences, U.S. Department of Energy.



7416 Hollister Avenue
Santa Barbara, CA 93117
+1 (805) 696-6466
AFM.info@oxinst.com